Drop breakup dynamics of dilute polymer solutions: Effect of molecular weight, concentration and viscosity

Samrat Sur, Jonathan Rothstein

University of Massachusetts Amherst, MA

Abstract

The large extensional viscosity of dilute polymer solutions has been shown to dramatically delay the breakup of jets into drops. For low shear viscosity solutions, the jet breakup is initially governed by a balance of inertial and capillary stresses before transitioning to a balance of viscoelastic and capillary stresses at later times. This transition occurs at a critical time when the radius decay dynamics shift from a 2/3 power law to an exponential decay as the increasing deformation rate imposed on the fluid filament results in large molecular deformations and rapid crossover into the elasto-capillary regime. By experimental fits of the elasto-capillary thinning diameter data, relaxation time less than one hundred microseconds have been successfully measured. In this paper, we show that, with a better understanding of the transition from the inertia-capillary to the elasto-capillary breakup regime, relaxation times close to ten microseconds can be measured with the relaxation time resolution limited only by the frame rate and spatial resolution of the high speed camera. In this paper, the dynamics of drop formation and pinch-off are presented using Dripping onto Substrate Capillary Breakup Extensional Rheometry (CaBER-DoS) for a series of dilute solutions polyethylene oxide in water and in a viscosified water and glycerin mixture. Four different molecular weights between 100k and 1M g/mol were studied with varying solution viscosities between 1 mPa.s and 22 mPa.s and at concentrations between 0.004 and 0.5 times the overlap concentration, c^*. The dependence of the relaxation time and extensional viscosity on these varying parameters were studied and compared to the predictions of dilute solution theory while simultaneously searching for the

lower limit in solution elasticity that can be detected. For PEO in water, this limit was found to be a fluid with a relaxation time of roughly 20 μs. These results confirm that CaBER-DoS can be a powerful technique characterizing the rheology of a notoriously difficult material to quantify, namely low-viscosity inkjet printer inks.

I. Introduction

The addition of a small amount of moderate to high molecular weight polymer to a Newtonian solvent can yield rather dramatic changes to the rheological behavior of the fluids. This is especially true in extensional flows where presence of polymers can significantly increase the resistance to stretching flows [1]. The resistance to extensional flows is characterized by the extensional viscosity of the fluid. For dilute solutions of high molecular weight polymers, the extensional viscosity can be several orders of magnitude larger than the shear viscosity. The effects of large extensional viscosity can be readily observed through the ability of these solutions to form persistent filaments and to delay the breakup into droplets when stretched [1-7]. This polymer-induced viscoelasticity has many industrial applications, including in inkjet printing. In inkjet printing, the addition of a small amount of polymer to the ink can help minimize satellite and daughter droplet formation which is essential for printing quality. However, the addition of too much polymer to the ink can make printing impossible by delaying breakup of ink jets into drops [8, 9].

The influence of polymers in inkjet printing fluids or other low-viscosity dilute polymer solutions is often difficult to see in standard shear rheology measurements. The shear viscosity often appears to be Newtonian in steady shear measurements and, in small amplitude oscillatory tests, the relaxation time is often so small (in the range of micro to milliseconds) that it is difficult to measure using standard rheometric techniques. However, for these micro-structured

fluids, the extensional viscosity, which is a function of both the rate of deformation and the total strain accumulated, is often clearly evident even if it is not readily measurable. Some of the most common manifestations of extensional viscosity effects in complex fluids can be observed in the dramatic increase in the lifetime of a fluid thread undergoing capillary break-up driven by interfacial tension. Depending on the composition of the fluid, viscous, elastic and inertial stresses may all be important in resisting the filament breakup resulting from capillary forces. The breakup dynamics can thus be used to obtain a number of fluid properties including the surface tension, σ, the shear viscosity, η, the extensional viscosity, η_E, and the relaxation time of the fluid, λ. Here, we will be using dripping onto substrate capillary breakup extensional rheometry (CaBER-DoS) developed by Dinic et al. [10, 11] to visualize and characterize the extensional rheology of dilute, low-viscosity polymer solutions.

In the past several decades, a number of measuring techniques have been used to characterize the extensional flow rheology of complex fluid. Of those techniques, filament stretching extensional rheometry (FiSER) and capillary breakup extensional rheometry (CaBER) techniques are the most common ones [1, 4, 12-15]. In both these techniques, a small amount of liquid is placed between two cylindrical discs or plates. In a filament stretching device, at least one of the cylindrical discs is driven in a controlled manner so that a constant extension rate can be imposed on the fluid filament while the stress response of the fluid to the stretching deformation is measured through a combination of a force transducer and a laser micrometer to measure the filament diameter [5, 16]. This technique is limited by the maximum strain that can be achieved ($\varepsilon_{\max} \approx 6$) and the maximum imposed deformation rates ($\dot{\varepsilon}_{\max} \approx 10\text{s}^{-1}$) that can be imposed. As a result, the use of FiSER is limited to mostly polymer melts or higher viscosity

polymer solutions where the zero shear rate viscosity is greater than approximately $\eta_0 > 1$ Pa.s [17].

In CaBER, a step strain is rapidly imposed on the fluid between the two plates by rapidly displacing the top plate by a linear motor over a short distance [18]. This extension produces a liquid filament between the two plates. The minimum diameter of the thinning filament is then measured as a function of time until break-up in order to calculate the apparent extensional viscosity and the relaxation time of the fluid. This is a common technique for determining the extensional rheology of viscoelastic fluids with viscosities as low as $\eta_0 = 70$ mPa.s and relaxation times as small as $\lambda = 1$ ms [19]. Along with the viscosity limit of the CaBER technique, another limitation of this method is the inertial effects resulting from the dynamics of the rapid step stretch imposed by the motor motion. At the high velocities required to measure the breakup dynamics of low viscosity fluids, the rapid step strain can lead to oscillations in the filament that make measurement of extensional rheology difficult. Recently Campo-Deano et al. [20] used a slow retraction method (SRM) to investigate filament thinning mechanisms of fluids with shear viscosities similar to water and very short relaxation times. This experimental technique involves slowly separating the pistons just beyond the critical separation distance for which a statically stable liquid bridge can exist. At this point, the filament becomes unstable and the thinning and breaking process is initiated. This SRM technique avoids inertial effects allowing the authors to extract relaxation times as short as $\lambda = 200$ μs for dilute aqueous solutions of polyethylene oxide (PEO) with a molecular weight of $M_w = 1 \times 10^6$ g/mol and shear viscosities between $1 < \eta_0 < 3$ mPa.s [20]. Vadillo et al. [19] have further pushed the limit by measuring relaxation times as short as $\lambda = 80$ μs by using a Cambridge Trimaster rheometer

(CTM) [21] along with a high speed camera with adjustable fps with reduction of frame size for a series of solution of monodisperse polystyrene dissolved in diethyl phthalate (DEP) with concentration of polystyrene ranging from dilute to concentrated with solution viscosity of $\eta_0 = 12$ mPa.s. More recently Greiciunas et al. [22] have used the Rayleigh Ohnesorge jetting extensional rheometer (ROJER) technique [23] to measure relaxation times of dilute solutions of PEO, with molecular weight $M_w = 3\times10^5$ g/mol mixed in 25%/75% (by weight) glycerol/water solution. The ROJER is one of the more technically challenging of all the extensional rheology methods for characterizing low viscosity fluids to implement. However, it does have the benefit of eliminating the need for high speed imaging which can reduce costs substantially. In their work, they were able to measure relaxation time as low as $\lambda = 102$ μs for a solution viscosity with zero shear viscosity of $\eta_0 = 2.9$ mPa.s. In this technique, fluid is jetted through a small diameter nozzle where a small perturbation is applied to drive a capillary instability along the liquid jet. The instability eventually grows large enough to cause the jet to break up into droplets downstream. A camera is used to capture the thinning dynamics from which the extensional rheology of the fluids can be calculated in much the same way as in CaBER.

Amazingly, there are industrial applications like inkjet printing which require devices that can experimentally characterize the extensional rheology of dilute solutions with relaxation times even lower than those described above. Recently, Dinic et al. [10] have developed a dripping onto substrate CaBER technique called CaBER-DoS which can measure relaxation times much less than $\lambda \approx 1$ ms for low viscosity fluids ($\eta_0 \approx 1$ mPa.s). In their experimental setup, a fluid dispensing system is used to deliver a drop of fluid at a relatively low flow rate onto a glass substrate placed at a fixed distance below the exit of the nozzle. As the droplet slowly drips from

the nozzle, a filament is formed. By capturing the droplet on the substrate and not allowing it to fall further, the filament is allowed to breakup under capillary action in much the same way that CaBER works. The advantage is that the inertia associated with the moving of the top plate is removed as are the acceleration and the velocity limit of the actuator. Additionally, compared to the slow retraction method, CaBER-DoS is much better suited for highly volatile fluid where evaporation can play a large role because the experiments are performed much more quickly. For visualization, a high-speed imaging system was used, with a frame rates varying from 8000 to 25,000 fps. Dinic et al. [10] performed a series of studies on aqueous solutions of PEO having a of molecular weight of $M_{\mathrm{w}} = 1\times10^{6}\,\mathrm{g/mol}$. In all their experiments, the concentration of PEO was kept within the dilute region. They demonstrated a dependence of relaxation time on concentration, *c*, for dilute, aqueous PEO solution as $\lambda_E \propto c^{0.65}$ rather than the expected $\lambda_E \propto c$ from dilute theory [24]. This deviation was attributed to the much lower concentration required in extensional flows for a fluid to truly be within the dilute regime [10]. In fact, Clasen et al. [2] showed that in extensional flows an ultra-dilute concentration below $c/c^*<0.01$ is needed to recover the expected relaxation times and scaling's for dilute systems. Here, c/c^* is the reduced concentration with c^* defined as the coil overlap concentration. Dinic et al. [10] were successfully able to measure relaxation times as low as $\lambda_{\mathrm{E}} \approx 0.3\,\mathrm{ms}$. In follow up papers, the authors further extended their technique by performing extensional rheometry measurements on various other complex fluids [25] such as glycerol-water mixtures, ketchup, mayonnaise, photovoltaic ink and semi-dilute solutions of poly-acrylamide. They were able to capture and differentiate between the inertio-capillary thinning, visco-capillary thinning and elasto-capillary thinning dynamics using the CaBER-DoS. Through this technique, Dinic et al. [11] captured the differences in the necking region for different fluids during pinch-off. For pure water, it was

observed that the necking region forms a cone close to pinch-off point as predicted by theory. For a polymer solution, a long cylindrical filament was formed and the pinch-off was found to occur in a location near the mid-plane of the filament. For a multicomponent complex fluid, such as shampoo, a non-slender liquid bridge was formed resulting in the formation of two axisymmetric cones after break-up. Through these initial studies, Dinic et al. [11] have established a quick, reliable method to perform extension rheometry on low-viscosity fluids while establishing the microstructured effects on the pinch-off dynamics.

In this paper, we extend the work into thinning dynamics of low viscosity, elastic fluids using the CaBER-DoS technique by systematically probing the effects of polymer molecular weight, solution viscosity and concentration down to the point at which measurements of extensional viscosity and relaxation time become limited by camera resolution. In this study, we focus on the transition between the early time inertia-capillary regime and late stage elasto-capillary regime. The sharpness of this transition allows us to measure the extensional rheology of these PEO solutions with very few data points. In fact, from the parametric studies performed here, we have developed a simple relation to determine the relaxation time of low concentration, low molecular weight and low viscosity polymer fluids by capturing a single image of fluid filament before breakup. Using this technique, we have demonstrated that relaxation time measurements as low as $\lambda_E = 20$ μs can be measured using the CaBER-DoS technique.

II. Materials

The low-viscosity elastic fluids tested in this work are dilute solutions of polyethylene oxide (PEO) (supplied by Aldrich Chemical Co.) with molecular weights ranging from $M_w = 1\times10^5$ to 1×10^6 g/mol in glycerol and water mixtures. In general, commercial PEO samples are known to be polydisperse. Tirtaamadja et al. [7] measured the polydispersity index

of the M_w=1×10^6 g/mol PEO sample used in their study to be PDI=1.8. Since our samples were purchased from the same supplier, we expected them to have similar polydispersity as those used in the works of Tirtaamadja et al. [7]. The polydispersity of the polymer can have an impact on measurements and comparisons to Zimm theory which assumes a perfectly monodisperse polymer sample. In this work, the polymer concentrations were varied, while keeping it below the coil overlap concentration, c^*, which was calculated using the definition provided by Graessley [26] such that $c^*=0.77/[\eta]$. Here $[\eta]$ is the intrinsic viscosity of the polymer solution which depends on the molar mass of the chain according to the Mark-Houwink-Sakurda equation $[\eta]=KM^a$, where K=0.072 cm^3/g and $a=0.65$ for PEO in water and glycerol [7]. To arrive at the value of these Mark-Houwink constants, Tirtaamadja et al. [7] used a linear regression analysis to obtain a line of best fit to all the previously published data for PEO in water and PEO in water/glycerol over a range of molecular weight spanning from 8x10^3<M_w<5x10^6 of PEO. They observed that all the data agreed well with each other and were within the experimental error for variation in the solvent composition. The concentration of PEO was varied from 0.004c^* to 0.5c^*. The glycerol and water mixtures were chosen such that the shear viscosity of the solution varied between $6\ \text{mPa.s} \le \eta_0 \le 22\ \text{mPa.s}$. The shear viscosity was measured using a cone and plate rheometer (DHR-3, TA instruments) and showed a constant shear viscosity over the shear rate range that could be probed by the rheometer ($1\ \text{s}^{-1} < \dot{\gamma} < 100\ \text{s}^{-1}$). The surface tension for each glycerol and water mixture was selected based on values available in the literature [27]. In preparing the solutions, water was first mixed with the required concentration of the PEO and mixed in a magnetic stirrer (CIMAREC) for 2 hours and then the required amount of glycerol was added, and again mixed for another 24 hours at 500 rpm at room

temperature. A table of the shear viscosity and surface tension of each solution tested is presented in Table S.1 (Supplementary).

III. Experimental Setup

The dripping onto substrate capillary breakup extensional rheometry (CaBER-DoS) setup is shown in Figure 1. CaBER-DoS requires a high speed camera (Phantom- Vision optics, V-4.2) to capture the filament break-up process, a liquid dispensing system (KD Scientific) to control the volume flow rate, a cylindrical syringe tip, a glass substrate and a high intensity light source. In CaBER-DoS, a liquid bridge is formed between the substrate and the nozzle by allowing a drop of liquid to drip from the nozzle onto the glass substrate. The height of the nozzle, H_0, from the substrate is selected such that an unstable liquid bridge is formed as soon as the drip makes contact and spreads on the substrate. In the experiments presented here, an aspect ratio of $H_0 / D_{nozzle} = 3$ was used. The high speed camera used for visualization can record at frame rates well over 100,000fps, but at those rates the number of pixels per image was quite small. For most of the measurements presented here a frame rate of 25,000 fps was used with a resolution of 192x64pixel^2. The magnification attained using Edmund optics long range microscope lens (EO-4.5x zoom) is 5μm/pixel. However, to minimize the effect of the resolution error (± 5μm) on the diameter values reported, we do not report data below a filament diameter length of $D_{filament} < 10$ μm even though the edge detection algorithm we used to capture the diameter decay (Edgehog, KU Leuven) has sub-pixel resolution. In order to calculate the extensional viscosity, the diameter decay was fit with a spline and then differentiated as described below. The diameter of the nozzle was $D_{nozzle} = 800$ μm and the volume flow rate of $Q = 0.02$ ml/min was maintained.

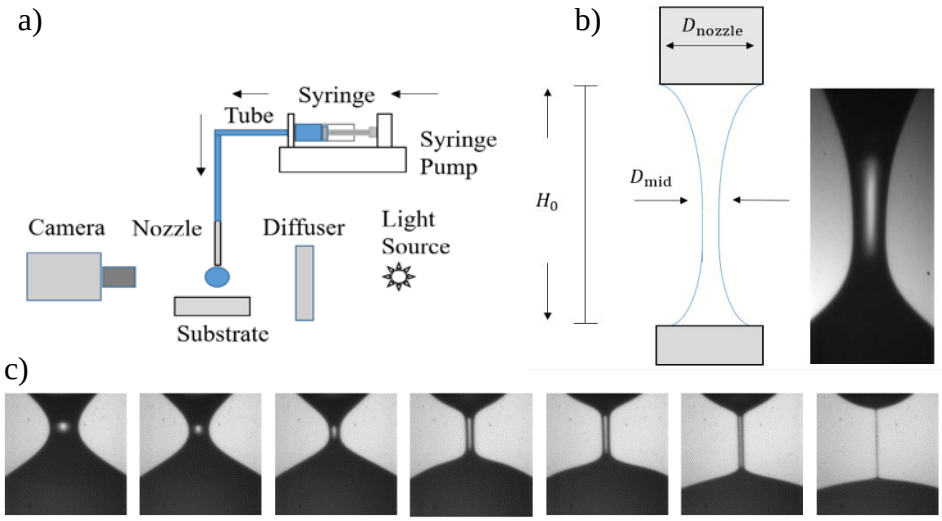

Figure 1. a) Schematic diagram of the drip onto substrate capillary breakup extensional rheometry (CaBER-DoS) setup with all the major components labeled and b) a magnified image of the filament formation between the exit of the nozzle and the substrate along with appropriate dimensions c) sequence of images showing the development of the filament and subsequent thinning.

IV. Methodology

The dynamics of the filament thinning of low viscosity fluids in the CaBER-DoS experiments presented here can be characterized by some of the well-defined physical models used to characterize the dynamics of drop formation for dilute polymer solutions from dripping nozzles [7] and continuous jets [28]. In this section, we will define some of the dimensionless numbers used to characterize the filament thinning dynamics along with the models used to categorize the thinning dynamics into three different regimes – inertio-capillary, visco-capillary and elasto-capillary. The three different regimes will be discussed below and highlighted in the results for different PEO solutions.

The driving force of the filament thinning in CaBER-DoS originates from the capillary pressure and depends, therefore, on the surface tension, σ, and the local curvature of the filament, $\kappa = 1/R_1 + 1/R_2$, where R_1 and R_2 are the principle radii of curvature on the filament. The capillary thinning is resisted by a combination of fluid viscosity, inertia, and elasticity depending on the fluid physical and rheological properties and the size of the filament. The important dimensionless groups characterizing this necking process are the Ohnesorge number, $Oh = \eta_0 / \left(\rho\sigma R\right)^{1/2}$, which represents a balance of the inertial and viscous forces for a slender filament; the intrinsic Deborah number, $De = \dfrac{\lambda}{\sqrt{\rho R_0^{\,3} / \sigma}}$, which represents the ratio of the characteristic relaxation time of the fluid to the timescale of the flow; and the elasto-capillary number, $Ec = \lambda_E \sigma / \eta_0 R_0$, which represents a ratio of the characteristic relaxation time of the fluid and the viscous timescale of the flow. In this case, the intrinsic Deborah number, $De = \lambda_E / t_R$, is a ratio of the extensional relaxation time of the fluid to the Rayleigh time, $t_R = (\rho R_0^{\,3} / \sigma)^{1/2}$. In these dimensionless groups, η_0 is the shear viscosity of the fluid, R_0 is the radius of the filament, σ is the surface tension, ρ is the density and λ_E is the relaxation time in extension. Clasen et al. [29] have shown that for Ohnesorge numbers less than $Oh < 0.2$, the thinning of the fluid filament will be dominated by a balance of inertial and capillary forces (inertia-capillary regime), while for $Oh > 0.2$, the thinning of the fluid filament will be dominated by a balance of viscous and capillary forces (visco-capillary regime). For a low Ohnesorge number flow, for $De > 1$, the thinning process will be dominated by a balance of elastic and capillary forces (elasto-capillary regime), while, for $De < 1$, elastic forces will play no role in the breakup dynamics [7]. Finally, for a large Ohnesorge number flow and an elasto-capillary number less

than $Ec < 4.7$ the filament thinning will remain visco-capillary while for $Ec > 4.7$ the flow will again transition to elasto-capillary thinning [29].

In the inertia-capillary regime, the radius decays with time following a 2/3 power law dependence [5],

$$\frac{R(t)}{R_0} = 0.64\left(\frac{\sigma}{\rho R_0^3}\right)^{1/3}(t_c - t)^{2/3} = 0.64\left(\frac{t_c - t}{t_R}\right)^{2/3}. \quad (1)$$

Here, t_c is the time at which the filament breaks up, R_0 is the initial radius and t_R is the Rayleigh time which is a characteristic timescale for the breakup of fluids in this inertia-capillary regime [10]. The prefactor in equation 1 has been reported to be between 0.64 and 0.8 with some experimental measurements finding values as large as 1.0 [5, 10, 20, 29]

For the visco-capillary regime, the radius decays linearly with time as shown by Papageorgiou [30],

$$\frac{R(t)}{R_0} = 0.0709\left(\frac{\sigma}{\eta_0 R_0}\right)(t_c - t) = 0.0709\left(\frac{t_c - t}{t_v}\right). \quad (2)$$

Here, $t_v = \eta_0 R_0 / \sigma$, is the characteristic viscous timescale for breakup.

For the elasto-capillary regime, the Entov [31] showed that, for an Oldroyd-B fluid, the radius will decay exponentially with time,

$$\frac{R(t)}{R_0} = \left(\frac{GR_0}{2\sigma}\right)^{1/3}\exp\left(-\frac{t}{3\lambda_E}\right). \quad (3)$$

Here, G is the elastic modulus of the fluid. Unlike the inertio-capillary regime where a conical filament is formed with two principle radii or curvature, in the elasto-capillary regime a cylindrical filament with a single radii of curvature is formed. In CaBER measurements, the extensional rheology of the fluid can be extracted from measurements of the diameter decay with time. The extension rate of the filament is given by

$$\dot{\varepsilon} = -\frac{2}{R_{\text{mid}}(t)}\frac{\mathrm{d}R_{\text{mid}}(t)}{\mathrm{d}t}. \tag{4}$$

Hence, for an Oldroyd-B fluid, the extension rate is constant, independent of time and only dependent on the fluids relaxation time, $\dot{\varepsilon} = 2/3\lambda_{\text{E}}$. The resulting filament decay has a constant Weissenberg number of $Wi = \lambda_{\text{E}}\dot{\varepsilon} = 2/3$. The Weissenberg number represents the relative importance of elastic to viscous stresses in a flow. This value is larger than the critical Weissenberg number of $Wi = 1/2$ needed to achieve coil-stretch transition and thus can be used to measure the extensional rheology of these polymer solutions. As seen in Equation 3, the relaxation time can be calculated from the slope of the log of the radius or diameter decay with time. In addition, the extensional viscosity can also be calculated from the measurement of diameter or radius decay with time,

$$\eta_{\text{E}} = \frac{\sigma / R_{\text{mid}}(t)}{\dot{\varepsilon}(t)} = -\frac{2\sigma}{\mathrm{d}R_{\text{mid}} / \mathrm{d}t}. \tag{5}$$

V. Results and Discussion

A. CaBER-DoS of PEO solutions with constant *c/c** and varying M_w and η_0

Throughout the results and discussion section, we will present CaBER-DoS results for a series of PEO solutions with varying solution viscosity, polymer molecular weight and concentration so that trends for each of these parameters can be identified and compared to theory. For most of the experiments presented here, the overarching goal was to extend the experimental characterization capabilities of CaBER-DoS to less and less elastic fluids. As we will demonstrate, this can be done either by extending the CaBER-DoS experimental capabilities or by finding trends with solvent viscosity, molecular weight or concentration that can be used to extrapolate from more elastic and measurable solutions to lower elasticity solutions that cannot

be characterized even in CaBER-DoS. In all cases, the concentration levels of the PEO were maintained in the dilute region, $c/c^* < 1$, where the results can be compared against theory.

In this subsection, we will focus on solutions with a fixed values of reduced concentration, c/c^*=constant for each polymer molecular weight. Although a wide spectrum of reduced concentrations were tested using CaBER-DoS, only a small subset of these concentrations will be systematically presented here. CaBER-DoS results are presented in Figures 2 and 3 for solutions of PEO with molecular weights of M_w= 1x10^6, 6x10^5, 2x10^5, and 1x10^5 g/mol and solution viscosity of η_0=6 mPa.s, 10 mPa.s and 22 mPas.

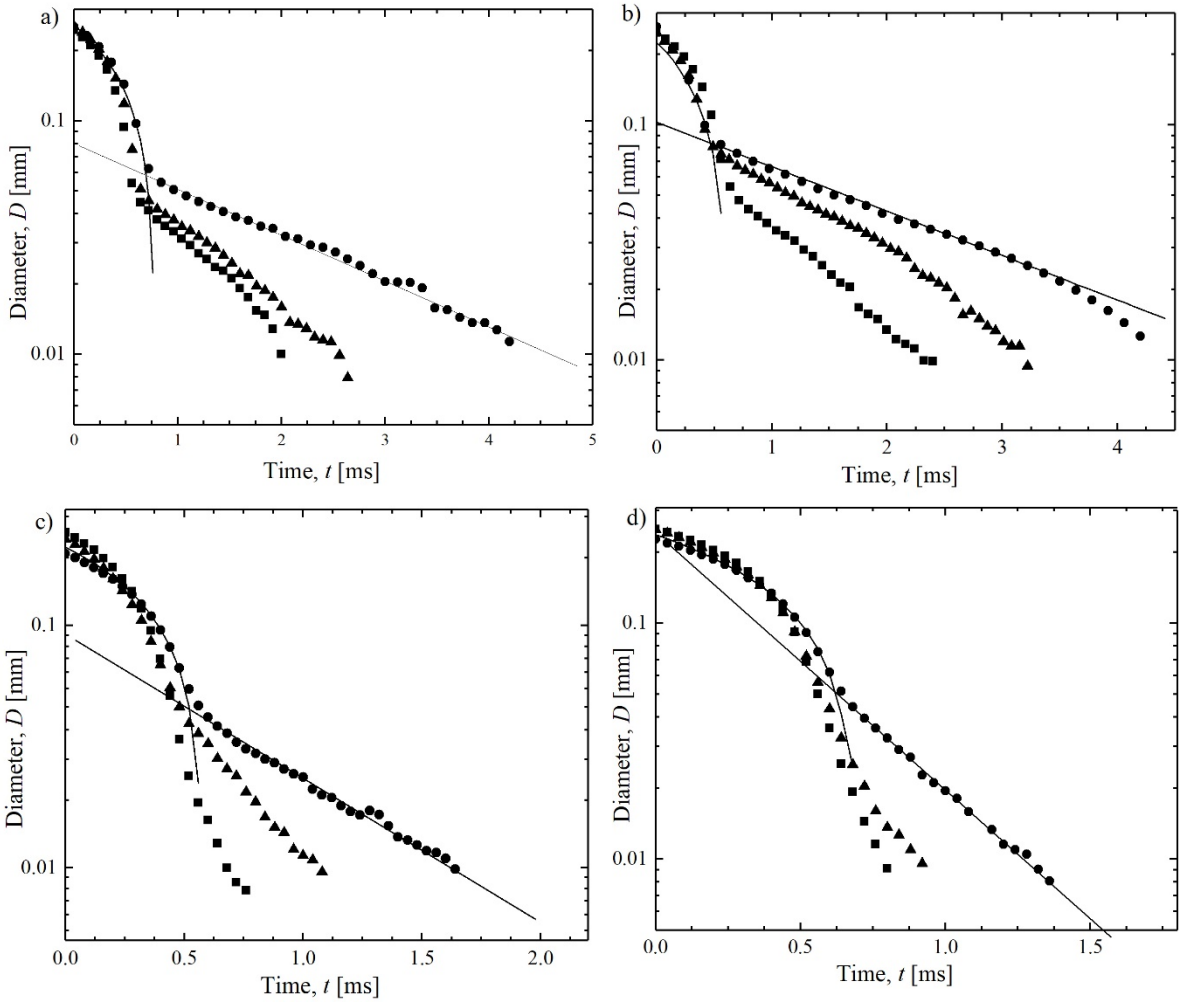

Figure 2. Plot of diameter, D, as a function of time, t, for a series of PEO solutions in glycerin and water with a) molecular weight of M_w =1x10^6 g/mol and a reduced concentration of

*c/c**=0.02, b) M_w =600k g/mol and *c/c**=0.03, c) M_w =200k g/mol and *c/c**=0.05, and d) M_w =100k g/mol and *c/c**=0.08. In each plot the solution viscosity is varied from η_0=6 mPa.s (■), to η_0=10 mPa.s (▲) and finally to η_0=22 mPa.s (●). Solid lines represent the inertia-capillary and elasto-capillary fits to the experimental data from theoretical predictions.

The diameter decay as a function of time is plotted in Figure 2 for each of the four different molecular weight PEO solutions tested. In each subfigure, the diameter decay is shown as a function of solution viscosity at a fixed reduced concentration. Note that the value of the reduced concentration presented increases with decreasing polymer molecular weight to insure that a transition to an elasto-capillary thinning could be observed even at the lowest solvent viscosity, $\eta_0 = 6$ mPa.s , for each molecular weight PEO. In all cases, the diameter evolution in time was found to exhibit two distinct regimes: an inertial capillary regime characterized by a decay of the diameter with a 2/3 power law with time followed by an elasto-capillary regime characterized by an exponential decay of the diameter with time. Late time deviation from the exponential decay in some data sets shows the effects of the finite extensibility of the polymer solution. A solid line was superimposed over one data set in each figure to demonstrate the quality of the fit to theoretical predictions of each of these regimes. Note that in these figures, the diameter decay begins at roughly D = 250 μm and not at the diameter of the initial filament which was close to the diameter of the nozzle, D = 800 μm. This was a result of the high optical magnification needed to capture the late time dynamics of the extremely fine filament and to characterize the extensional rheology of the fluid.

As can be observed from Figure 2, the transition from the initial power law decay to the late stage exponential decay was extremely sharp in all cases with no more than one or two data points spanning less than one millisecond within this transition regime. In the section that follows, the sharpness of this transition will be utilized to significantly enhance the resolution

and sensitivity of relaxation time measurements from CaBER-DoS. The transition from an inertia-capillary to an elasto-capillary response is due to the growth of elastic stresses within the fluid filament as it was stretched over time. Within the inertia-capillary regime, the extension rate of the fluid filament increases with time such that $\dot{\varepsilon} = 4/\left(3\left(t_c - t\right)\right)$. At early times during the stretch, the extension rate is too small to deform the polymer within the solution because the Weissenberg number is less than one half, $Wi < 1/2$. As a result, in this regime, the elasticity of the fluid plays no role in the breakup dynamics. However, as the time approaches the cutoff time, t_c, the extension rate can grow large enough such that the Weissenberg number becomes larger than $Wi > 1/2$ and the polymer chain can begin to deform and build up elastic stress which will resist the extensional flow and dominate the breakup dynamics. In CaBER-DoS, theoretical predictions suggest that the elasto-capillary breakup should occur with a constant Weissenberg number of $Wi < 2/3$. Using this Weissenberg number, one can set an extension rate of $\dot{\varepsilon} = 2/3\lambda$ as the theoretical criteria for the transition from the inertia-capillary to the elasto-capillary regime. Doing this, a critical radius for the transition to the elasto-capillary regime was found. This is a reasonable first approximation, but, as will be discussed in detail in later sections, this critical radius over predicts the actual transition radius by a factor of approximately five times because it assumes that buildup of extensional deformation and stress in the polymer is instantaneous when in reality a finite amount of strain is required to build up sufficient elastic stress to surpass the inertial forces and become the dominant resistance to the capillary forces [32]. That being said, once the flow becomes elasto-capillary, given enough data points, the diameter decay can be used to characterize both the extensional viscosity and relaxation time of the PEO solutions as described in the previous section. An important observation that one can make from Figure 2 is that increasing either the molecular weight of the polymer or the solution

viscosity leads to an increase in breakup time of the filament due to an increase in the relaxation time of the polymer solution. Note also that the inertia-capillary dynamics, which manifest

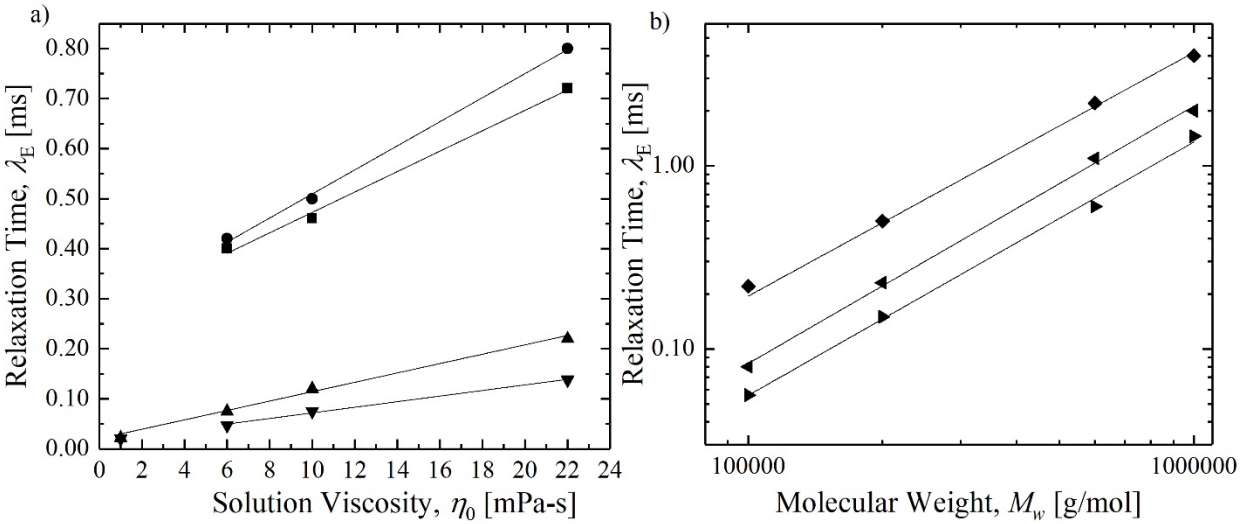

before the transition point, appears to be nearly independent of concentration. This variation in the relaxation time is plotted as a function of solutions viscosity and molecular weight in Figure 3.

Figure 3. Plot of extensional relaxation time, λ_E, as a function of solution shear viscosity, η_0, and molecular weight, M_w, for a series of PEO solutions in glycerin and water with a) molecular weight of M_w =1x10^6 g/mol and a reduced concentration of c/c^*=0.02 (■), M_w =600k g/mol and c/c^*=0.03 (●), M_w =200k g/mol and c/c^*=0.05 (▲) and M_w =100k g/mol and c/c^*=0.08 (▼) and b) solution viscosity of η_0=6 mPa.s and c/c^*=0.5 (♦), η_0=6 mPa.s and c/c^*=0.1 (◄) and η_0=1 mPa.s and c/c^*=0.5 (►). Solid lines represent the fits to the experimental data.

For the case of PEO with a molecular weight of $M_w = 1\times10^6$ g/mol, the relaxation time for a solution viscosity with shear viscosity of $\eta_0 = 6$ mPa.s was found to be $\lambda_E = 0.4$ ms. The relaxation time increased to $\lambda_E = 0.72$ ms as the shear viscosity of the solution was increased to $\eta_0 = 22$ mPa.s. Similarly, for PEO with molecular weight of $M_w = 600$k g/mol, the relaxation time for a solution with a shear viscosity of $\eta_0 = 6$ mPa.s was found to be $\lambda_E = 0.42$ ms and $\lambda_E = 0.8$ ms for a solution with a shear viscosity of $\eta_0 = 22$ mPa.s. A reduction of close to a

factor of four was observed for the relaxation times measured for the lower molecular weights polymer solutions as compared to the higher molecular weights polymer solutions. Similar trends were observed for the lower molecular weights polymer solutions where for the case of PEO with molecular weight of $M_w = 100\text{k g/mol}$, the relaxation time for a solution with shear viscosity of $\eta_0 = 6$ mPa.s was found to be $\lambda_E = 0.045$ ms. The relaxation time increased to $\lambda_E = 0.13$ ms as the shear viscosity of the solution was increased to $\eta_0 = 22$ mPa.s. From theory it has been shown that the relaxation time of a dilute polymer solution should increase linearly with the viscosity as shown in equation 6, a linear increase with solvent viscosity was observed for all of our experimental measurements. According to kinetic theory, the longest relaxation time of an isolated polymer coil in dilute solution is proportional to the solvent viscosity as [2, 6]

$$\lambda_z = \frac{1}{U_{\eta\tau}} \frac{[\eta]\eta_s M_w}{RT}. \tag{6}$$

Where $U_{\eta\tau} = \lambda_\eta / \lambda_0$ is the universal ratio of the characteristic relaxation time of a dilute polymer solution system λ_η and the longest relaxation time λ_0. In addition, M_w is the molecular weight, η_s, is the solvent viscosity, $[\eta]$ is the intrinsic viscosity, R is the universal gas constant and T is the absolute temperature. The numerical value of the universal ratio depends on the relaxation spectrum of the specific constitutive model [2]. Given the molecular weight dependence of the intrinsic viscosity for PEO in water and glycerol as shown earlier, the Zimm model can be used to compare the dependence of the relaxation time on the molecular weight of the PEO. For a constant solvent viscosity, the relaxation time for the PEO should scale with molecular weight as $\lambda_z \propto M_w^{1.65}$. In our experiments, a power law dependence of $\lambda_E \propto M_w^{1.4}$ was observed. This value is close, but does not precisely match the predictions of the Zimm theory as seen in Figure 3b. It

is important to note that a similar discrepancies between the Zimm theory and experimental measurements have been observed in the past by Tirtaamadja et al. [7] and others. In their experiments, the relaxation time of a series of different molecular weights of PEO in glycerol/water mixtures was measured by monitoring a droplet formation from a nozzle due to gravity. Although they do not quantify it, a scaling of $\lambda_{Eff} \propto M_w^{1.2}$ can be fit to their data. As with the measurements here, the measured value of the power-law coefficient was less than the value predicted by the Zimm model. As we will discuss in detail later, this discrepancy is likely due to the fact that even though these solutions all have polymer concentrations less than coil overlap concentration, c^*, they are not truly dilute in extensional flows until the reduced concentration is below $c/c^*<10^{-4}$ [2]. Thus the Zimm scaling in Equation 6 may not hold in extensional flows until the concentration becomes extremely small, $c/c^*<10^{-4}$.

The effect of solution viscosity on the evolution of the apparent extensional viscosity, η_E, as a function of strain, ε, can be found in Figure 4. An important point to note here is that the strain reported in figure 4, which is defined as $\varepsilon = 2\ln(R_0 / R(t))$, depends heavily on the value of the initial radius, R_0, used to define it. The strain therefore requires a consistent and repeatable choice for R_0. One possibility is to choose the radius of the syringe tip which can be made a priori without knowledge of the fluid rheology. Here, however, we chose to use the radius at which the dynamics of the filament decay begins to transition from an inertia-capillary to an elasto-capillary flow. This transition point is defined as the radius at which the Weissenberg number becomes greater than Wi = ½. This is a more physically correct choice for R_0 because, at larger radii, the Weissenberg number is less than Wi < ½ and no appreciable strain is accumulated in the polymer chains. However, for radii smaller than $R < R_0$, strain is

continuously accumulated in the polymer chains up until the point of filament failure. Using equations 1, 3 and 4, a value for R_0 becomes $R_0 = 1.23\left(\lambda_E \sigma / \rho\right)^{1/3}$ [6, 19, 20]. The only downside to this choice is that extensional relaxation time of the fluid must be measured from the data before the strain can be determined, however, because all the data presented here had a measurable relaxation time, this was not an issue.

In Figure 4, an increase in the extensional viscosity was observed with increasing strain for all solutions tested. At large strains, the extensional viscosity in each case approached a steady-state value signifying that the polymer chains had reached their finite extensibility limit. At this point, the resistance to filament thinning is not viscoelastic but rather returns to a viscous response albeit with a viscosity several orders of magnitude larger than the zero shear viscosity [19]. For the case of PEO with molecular weight of $M_w = 1\times10^6$ g/mol, a steady state extensional viscosity of $\eta_E = 8$ Pa.s and $\eta_E = 3$ Pa.s were observed for a solution with shear viscosities of $\eta_0 = 22$ mPa.s and $\eta_0 = 6$ mPa.s respectively. The resulting Trouton ratio, $Tr = \eta_E / \eta_0$, was between $Tr \approx 400$ and $Tr \approx 500$ for all the high molecular weight PEO solutions tested. This value is much larger than the Newtonian limit of Tr =3 showing the degree of strain hardening by these high M_w PEO solutions. Additionally, the roughly linear increase the value of the steady state extensional viscosity with increasing solution viscosity was observed for each of the different molecular weight PEOs tested. The result was a collapse of the data when the Trouton ratio was plotted as a function of Hencky strain for a given molecular weight obtained at fixed concentration but variable shear viscosity. This data is presented in supplementary material Figure S.2. These trends with solvent viscosity conform to the predictions of the FENE-P model as long as the value of the steady state Trouton ratios are significantly larger than Tr =3.

Note that in Figure 4, both the reduced concentration and the molecular weight were varied between subfigures. Here, the reduced concentration of the lowest molecular weight samples was purposefully increased in order to obtain coherent filaments from which clean extensional viscosity measurements could be extracted. In fact, unlike the $M_w = 1\times10^6$ g/mol PEO solutions at *c/c**=0.02, measurements of extensional rheology for the $M_w = 100$k g/mol at *c/c**=0.02 did not result in the formation of a viscoelastic filament, but broke up without transitioning from an inertia-capillary decay. Thus a natural lower limit in the measurable extensional viscosity of about $\eta_E = 0.1$ Pa.s was obtained, although we will show in the sections that follow that this is not truly a lower limit on extensional viscosity, but a lower limit on extensional relaxation time as the transition radius described above gets smaller and smaller with

decreasing extensional relaxation time and eventual becomes so small that it cannot be resolved optically.

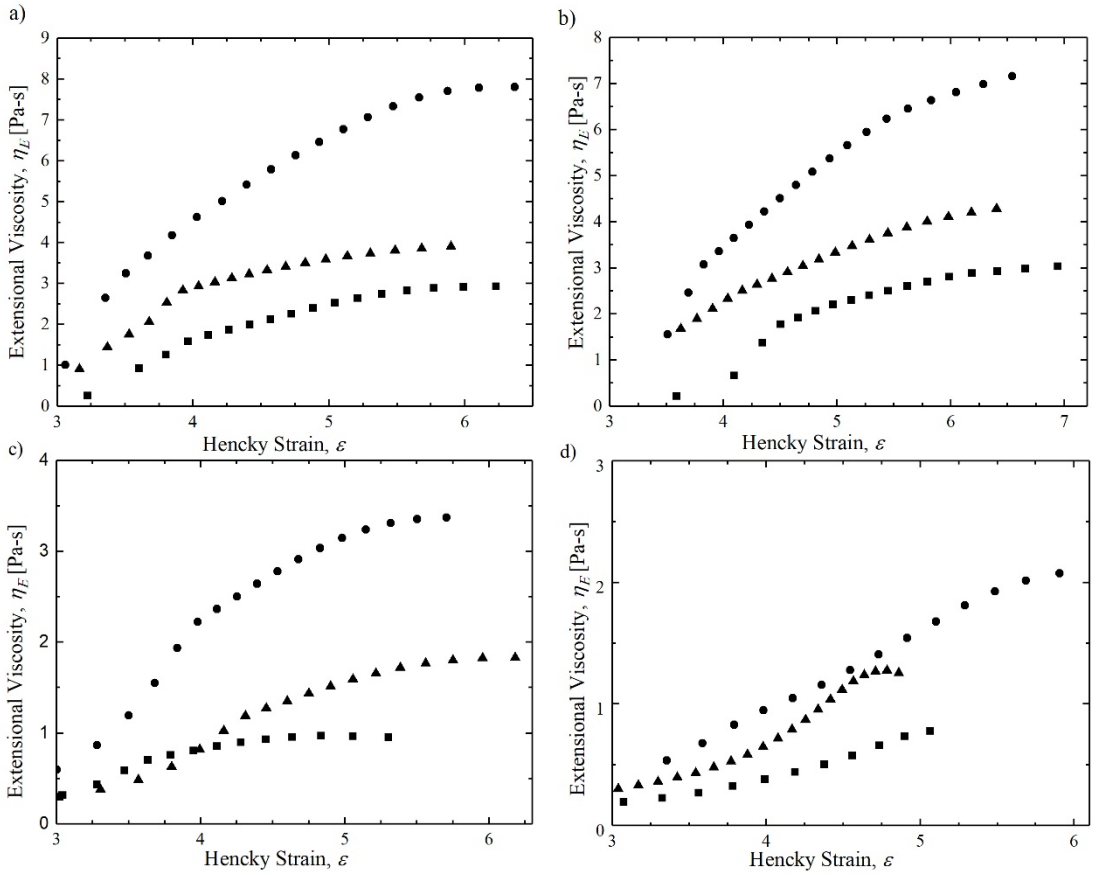

Figure 4. Plot of extensional viscosity, η_E, as a function of strain, ε, for a series of PEO solutions in glycerin and water with a) molecular weight of M_w =1x10^6 g/mol and a reduced concentration of c/c^*=0.02, b) M_w =600k g/mol and c/c^*=0.03, c) M_w =200k g/mol and c/c^*=0.05 and d) M_w =100k g/mol and c/c^*=0.08 at solution viscosity of η_0=6 mPa.s (■), η_0=10 mPa.s (▲) and η_0=22 mPa.s (●)

B. CaBER-DoS of PEO solutions with a fixed solution viscosity η_0 = 6 mPa.s and varying *c/c and M_w**

Similar to the discussions in the last section, CaBER-DoS results for a series of PEO solutions with varying polymer concentration and molecular weight are presented in this section so that trends for each of these parameters can be identified and compared to theory. Once a relation has been established, the relationship can be used to extrapolate the data to lower concentration or lower M_w solution which are not measurable using CaBER-DoS technique. In all cases, the concentration levels of the PEO were maintained in the dilute region, $c/c^* < 1$, so that the results could be compared against dilute theory. In this subsection, results are presented for values of reduced concentration varying from, c/c^*=0.004 to 0.5, but with the shear viscosity fixed at $\eta_0 = 6$ mPa.s . A small subset of the CaBER-DoS results are presented in Figures 5 and 6 for solutions of PEO with each sub figure corresponding to a fixed molecular weights of M_w = $1x10^6$, $6x10^5$, $2x10^5$, and $1x10^5$ g/mol.

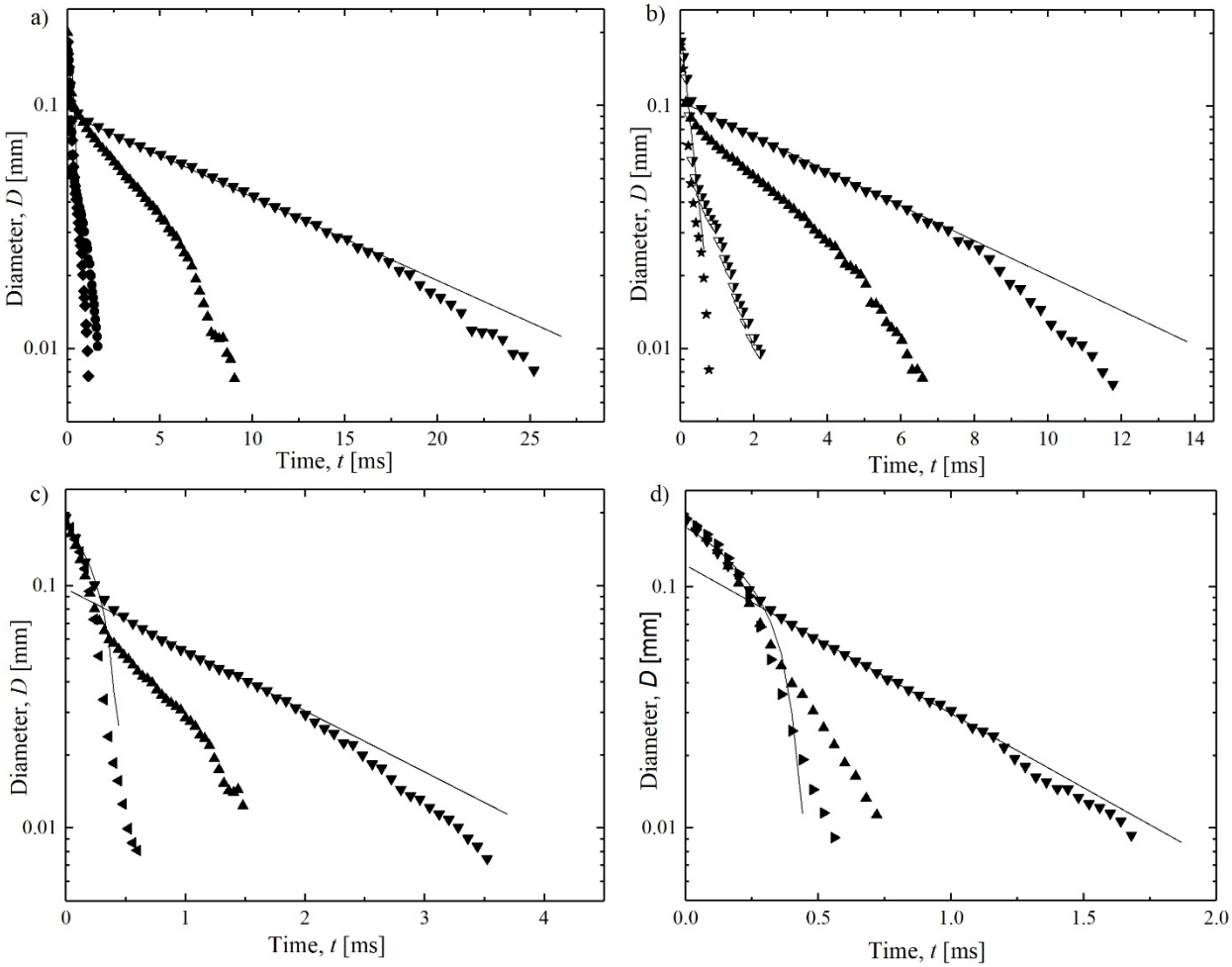

Figure 5. Plot of diameter, D, as a function of time, t, for a series of PEO solutions in glycerin and water at a fixed solution viscosity of η_0=6 mPa.s and molecular weight varying from a) M_w =1x10^6 g/mol, b) M_w =600k g/mol, c) M_w =200k g/mol and d) M_w =100k g/mol. In each subfigure, reduced concentration is varied from c/c^*=0.004 (♦), c/c^*=0.005 (✯), c/c^*=0.02 (●), c/c^*=0.03 (▼), c/c^*=0.05 (◀), c/c^*=0.08 (▶), c/c^*=0.1 (▲) and c/c^*=0.5 (▼). Solid lines represent the inertia-capillary and elasto-capillary fits to the experimental data from theoretical predictions.

The diameter decay as a function of time is plotted in Figure 5 for each of the four different molecular weight PEO solutions tested. In each subfigure, the diameter decay is shown as a function of reduced concentration at a fixed solution viscosity. For a given molecular weight, an increase in the reduced concentration was found to result in an increase in both the relaxation time and, subsequently, the time required for the filament to breakup. The increased

relaxation time can be seen qualitatively as a decrease in the slope of the linear region of the data in this semi-log plot. The breakup times of the filaments were greatly affected by both the concentration and molecular weight. For the highest molecular weight PEO tested, the breakup times were an order of magnitude larger than the lowest molecular weights PEO tested at the same reduced concentration. The sensitivity of the break up time to change in concentration was not as strong as to molecular weight. For instance, a tenfold increase in the breakup time could be induced by increasing the molecular weight by a factor of roughly six at a given reduced concentration. However, to achieve the same tenfold increase in the break up time at a fixed molecular weight required an increase in the reduced concentration by a factor of one hundred.

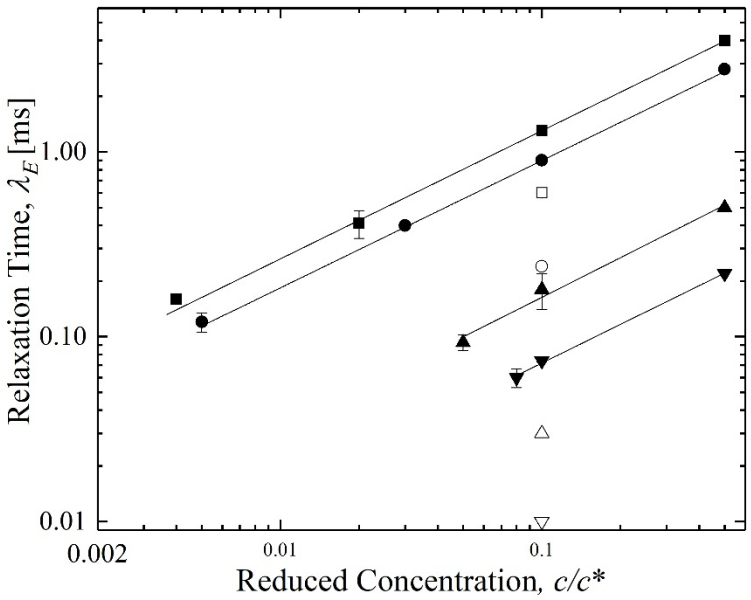

Figure 6. Plot of extensional relaxation time, λ_E, as a function of reduced concentration, c/c^*, for a series of PEO solutions in glycerin and water at fixed shear viscosity of η_0=6 mPa.s with a molecular weight of M_w =1x10^6 g/mol (■), M_w =600k g/mol (●), M_w =200k g/mol (▲) and d) M_w =100k g/mol (▼). Solid lines represent a power law fit to the data having the form λ_E ~(c/c*)$^{0.7}$. The hollow symbols shows the Zimm time at η_0=6 mPa.s for the molecular weight of (□) M_w =1x10^6 g/mol, (○) M_w =600k g/mol, (Δ)M_w =200k g/mol and (∇) M_w =100k g/mol.

In Figure 6, the relaxation time, λ_E, is presented as a function of reduced polymer concentration, c/c^*, for a series of PEO solutions in glycerin and water at a fixed shear viscosity of η_0=6 mPa.s. One can observe that, with an increase in the reduced concentration, an increase in the relaxation time was observed. For the case of PEO with molecular weight of $M_w = 1\times10^6$ g/mol, the relaxation time increased from λ_E=0.16 ms to 0.4 ms as the reduced concentration was increased from $c/c^* = 0.004$ to 0.5. These relaxation times are similar to those measured by Dinic et al. [10, 11] using the CaBER-DoS technique for a similar $M_w = 1\times10^6$ g/mol aqueous PEO solution. Note that below a concentration of c/c^*=0.004, a

viscoelastic filament could not be observed given the limitations in the temporal and spatial resolution of our high speed camera. Similar trends observed for each of the different molecular weight PEO solutions tested. With increasing molecular weight, the relaxation time measured for a given concentration was found to decrease. Additionally, the minimum concentration that could be characterized using CaBER-DoS was found to increase quite significantly with decreasing molecular weight as the cut-off appears to be limited by a minimum relaxation time of just below $\lambda_{\min} \approx 100\mu s$ that can be confidently characterized using CaBER-DoS.

For the case of PEO with molecular weight of $M_w = 100$k g/mol, the relaxation time was found to increase from λ_E =0.06 ms to 0.22 ms as the reduced concentration was increased from $c/c^* = 0.08$ to 0.5. For this molecular weight, the minimum concentration that could be characterized in CaBER-DoS was twenty times larger than that of the highest molecular weight sample. The increase in the relaxation time for all the different molecular weights PEO solutions tested was found to have power law dependence on the reduced concentration such that $\lambda_E \propto (c/c^*)^{0.7}$. Similar observation were made by Dinic et al. [10] where they observed a power law dependence of relaxation time on reduced concentration as $\lambda_E \propto (c/c^*)^{0.65}$ for their set of measurements on a series of aqueous PEO solution of a single molecular weight of, $M_w = 1\times10^6$ g/mol [10]. Tirtaamadja et al. [7] also observed a power law dependence of the relaxation time on reduced concentration as $\lambda_E \propto (c/c^*)^{0.65}$ for their set of measurements on a series of PEO in water/glycerol solution. This observation is counter-intuitive because according to equations 6 and 7, the relaxation time of isolated coils within dilute solution should be independent of the concentration. Clasen et al. [2] also noted a dependence of the longest relaxation time in extension on the reduced concentration, *c/c**. They rationalized this by noting

that the polymer viscosity can have a concentration dependence depending on the model used. For instance, using the Martin equation, Clasen et al. [2] were able to fit the relaxation time data to an exponential dependence on the reduced concentration predicted by the Martin equation. This model also showed that the concentration dependence should disappear as one moves farther and farther from the critical overlap concentration into the ultra-dilute regime where the relaxation time measurement was found to approach the Zimm relaxation time. Compared to the results of Clasen et al. [2], the range of concentrations for our working fluids in Figure 6 may be too narrow to observe a true dilute response as the data in Figure 6 do not appear to reach an asymptotic limit. From Clasen et al. [2], it is clear that only for reduced concentrations less than $c/c^* < 10^{-4}$ can a truly dilute value of the extensional relaxation be recovered. Thus, even though under quiescent conditions all of the PEO solutions studied in the present work were well within the dilute regime, $c/c^* < 1$, when deformed by an extensional flow the fluids all appear to exhibit semi-dilute solution behavior. This semi-dilute behavior arises from chain-chain interactions resulting from the increase in pervaded volume of the stretched chain. Thus, even though $c/c^* < 1$, excluded volume interaction between neighboring chains can become important. Using semi-dilute theory [33], Dinic et al. [10] showed through an alternate theoretical approach to Clasen et al. [2] that a power law dependence similar to that observed experimentally here, $\lambda_E \propto (c/c^*)^{0.7}$, could be rationalized.

An important final observation from Figure 6 should be made. From Figure 6 it is clear that the measured relaxation time do not asymptote to the Zimm relaxation time as the concentration was reduced. For the low molecular weight cases, M_w =100k g/mol and 200k g/mol, all the values of the measured relaxation time were larger than the Zimm relaxation time. However, for both the higher molecular weight PEOs cases, M_w =1x10^6 g/mol and 600k g/mol,

the measured relaxation times were found to decrease with decreasing concentration and, at the lowest concentrations tested, were measured to be smaller than the Zimm relaxation time. For the case of M_w =1x10^6 g/mol and 600k g/mol, the Zimm relaxation time is λ_z=0.6 ms and λ_z=0.24 ms respectively for reduced concentrations less than c/c^*<0.01. The value of the Zimm relaxation time for all the fluids tested here are presented in Table 1. Note that there are a number of differences between these CaBER experiments and the conditions under which the Zimm model predictions of relaxation time are made. First, the relaxation time predicted by the Zimm model is the shear relaxation time and these measurements are of the extensional relaxation time. Second, and perhaps more importantly, the Zimm model predictions assume a small deformation of the polymer chains, while the extensional flow studied here can result in a nearly fully extended polymer chain. Thus, it is not unreasonable to expect that differences would be observed between the Zimm relaxation time and the extensional relaxation time measured through CaBER.

It is important to note here that these relaxation time measurements do not appear to be in error. Each experiment were repeated multiple times and the exponential fits to the data used to determine the relaxation times were fit to between 10-20 pts of data over nearly a decade of time and diameter variation. Clasen et al. [2] observed similar trend and argued that for the cases where $\lambda_E < \lambda_z$ that the data was interpreted incorrectly. They fit their data with the assumption that the finite extensibility limit had been reached during the inertia-capillary decay and thus the relaxation time measurement were in error. Unfortunately, this argument does not hold for our data for several reasons. As seen in Figure 7, the filaments in our experiments, even as the relaxation time was found to drop below that predicted by the Zimm model, bore the expected cylindrical shape of an elasto-capillary thinning.

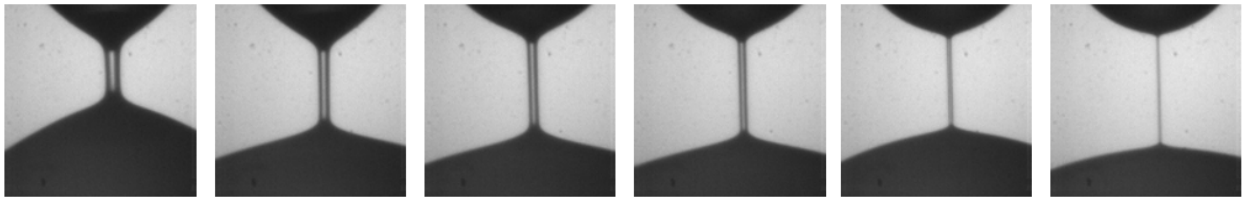

Figure 7. A sequence of images showing the formation of a slender filament and subsequent thinning for a PEO of M_w =1x10^6 g/mol at c/c^*=0.02 and shear viscosity of η_0=6 mPa.s.

In addition, following the experimental decay in the diameter as in Figures 2 and 5, a deviation was observed at late time which is clearly the onset of the finite extensibility limit well after the relaxation time has been fit to the data. Finally, it should be noted that all of the concentrations used in our experiments were an order of magnitude higher than the theoretical minimum concentration, c_{low}, above which theory predicts that a true elasto-capillary balance should be observable [19]. We are thus confident in the measurements of relaxation time and note that similar values of relaxation times in extensional flows have been observed in the past both in Clasen et al. [2] and Bazilevskii et al. [34]. The reason for these observations is still not fully understood, but requires further theoretical development along with and further experimental testing and development of this and other techniques to probe smaller and smaller concentrations and extensional relaxation times.

Molecular Weight M_w =1x10^6 g/mol		Molecular Weight M_w =600k g/mol		Molecular Weight M_w =200k g/mol		Molecular Weight M_w =100k g/mol	
Solution Viscosity [mPa.s] η_0	Zimm time, λ_z [ms]	Solution Viscosity [mPa-s] η_0	Zimm time, λ_z [ms]	Solution Viscosity [mPa-s] η_0	Zimm, time, λ_z [ms]	Solution Viscosity [mPa-s] η_0	Zimm time, λ_z [ms]
				1	0.006	1	0.0016
6	0.6	6	0.27	6	0.03	6	0.01
10	1.1	10	0.45	10	0.06	10	0.018
22	2.4	22	0.95	22	0.14	22	0.04

Table 1. Zimm relaxation times for the PEO solutions.

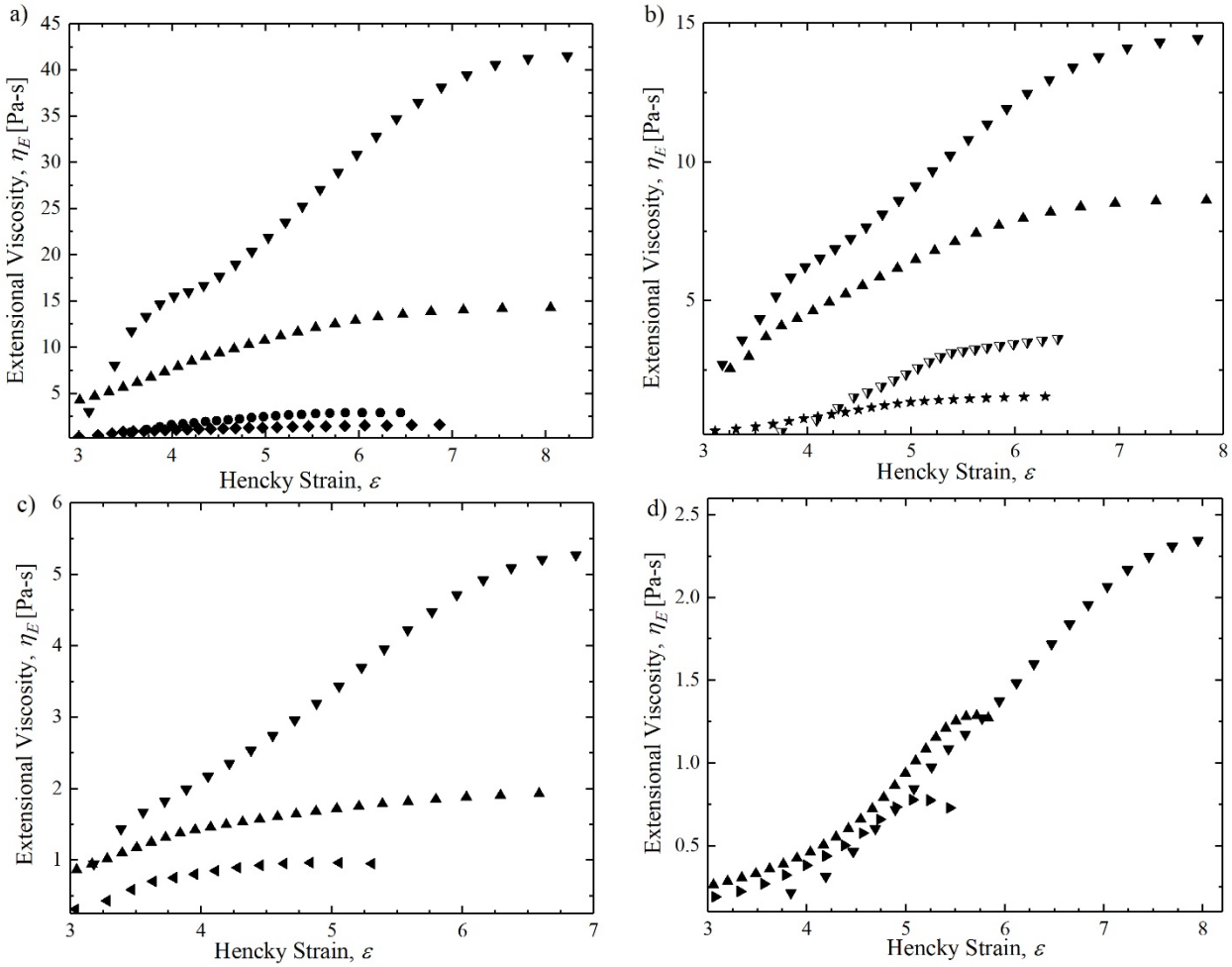

Figure 8. Plot of extensional viscosity, η_E, as a function of Hencky strain, ε, for a series of PEO solutions in glycerin and water at fixed shear viscosity of η_0=6 mPa.s with a molecular weight of a) M_w =1x10^6 g/mol, b) M_w =600k g/mol, c) M_w =200k g/mol and d) M_w =100k g/mol. The reduced concentration is varied from *c/c**=0.004 (♦), *c/c**=0.005 (✯), *c/c**=0.02 (●), *c/c**=0.03 (▽), *c/c**=0.05 (◄), *c/c* *=0.08 (►), *c/c**=0.1 (▲) and finally to *c/c**=0.5 (▼).

In Figure 8, the extensional viscosity, η_E, is plotted as a function of Hencky strain, ε, for a series of PEO solutions in glycerin and water at fixed shear viscosity of η_0=6 mPa.s and varying reduced concentration, *c/c** and molecular weights, M_w. In all cases, a steady-state extensional viscosity was reached at large values of Hencky strain. For the case of PEO with molecular weight of M_w=1x10^6 g/mol, the steady-state extensional viscosity observed varied

from η_E =1 Pa.s to 40 Pa.s as the reduced concentration was varied from *c/c**=0.004 to 0.5. Trouton ratios in the range of $Tr = 10^2 - 10^4$ are observed for the highest molecular weight PEO. Similar variations were observed for all the molecular weight tested. For the case of lowest molecular weight PEO tested, $M_w = 100\text{k g/mol}$, the steady state extensional viscosity observed varied from $\eta_E = 0.7$ Pa.s to 3 Pa.s as the reduced concentration was varied from *c/c**=0.08 to 0.5. This corresponds to Trouton ratios of the order of roughly $Tr \approx 10^2$. As observed from the diameter decay in Figure 5, at later times a deviation from the viscoelastic exponential fit was observed. As seen in Figure 8, this deviation was the result of the polymer chain approaching finite extensibility limit where the resistance to thinning returns to a viscous response albeit at a much higher viscosity.

C. A method for extending CaBER-DoS to make micro-seconds relaxation time measurements

In this section, a new approach to extend CaBER-DoS beyond the inherent limitations of the technique in order to make relaxation time measurements on the order of micro-seconds by taking advantage of the sharp transition between the inertia-capillary dominated thinning at early time and the elasto-capillary dominated thinning at later times is presented. As shown in the previous sections, CaBER-DoS can measure relaxation times greater than λ_E =0.1 ms without running into any temporal or spatial resolution limits of the chosen high speed camera. This is true independent of the solutions shear viscosity. However, the relaxation times were driven down even further by decreasing the shear viscosity of the solution or decreasing molecular weight of the polymers. The resulting rheological measurements were limited by the temporal resolution which limited the number of data points that could be captured in the elasto-capillary

region and the spatial resolution which limited the minimum size filament that could be accurately resolved. To directly measure the relaxation time, an exponential decay must be fit to the diameter decay data in the elasto-capillary thinning regime. In order for this fit to be accurate, a minimum of 5-10 data points is required. Here we show that a full exponential fit is not necessary to measure the relaxation time. In fact, in order to make relaxation time measurements for extremely low viscosity-low elasticity solutions only a single data point in the elasto-capillary region needs to be captured, thus increasing the resolution of CaBER-DoS by a full order of magnitude. This extension of CaBER-DoS takes advantage of the sharp transition between the inertia-capillary and the elasto-capillary thinning to define an experimentally observed transition radius, R^*. By calibrating the experimentally observed transition radius against the transition radius predicted from theory, R^*_{theory}, we demonstrated that an empirical correlation between the experimentally observed transition radius and the relaxation time can be formed. This finding significantly enhanced the resolution and sensitivity of the relaxation time measurements obtainable through CaBER-DoS.

Thinning dynamics of low viscosity dilute polymer solutions with Ohnesorge number, Oh<0.2 are known to be dominated by inertial decay [29]. As the diameter decays, the extension rates can eventually become large enough that the polymer chains to under-go a coil-stretch transition. This is known to occur for Weissenberg numbers greater than Wi >1/2. At these Weissenberg numbers, elastic stresses will grow with increasing accumulated strain. As they grow, the elastic stresses will become increasingly important to the flow and will eventually dominate the breakup dynamics of the liquid bridge [29]. In a CaBER experiments of an Oldroyd-B fluid, the thinning dynamics of the liquid bridge are known to occur at a constant Weissenberg number of Wi = 2/3. Thus, a reasonable approach taken by a number of previous

groups [6, 19, 20] to determine the transition point is to assume that the transition from inertio-capillary to elasto-capillary flow occurs when the extension rate induced by the intertio-capillary flow grows to $\dot{\varepsilon} = 2/3\lambda_E$. Using this value of the extension rate in combination with Equations 1 and 4, a relation for the theoretical transition radius can be obtained,

$$R^*_{\text{theory}} = 1.01\left(\frac{\lambda_E{}^2\sigma}{\rho}\right)^{1/3}. \tag{7}$$

If equation 7 is valid, the extension relaxation time can be estimated by measuring the initial radius of the cylindrical filament that is characteristic of the elasto-capillary flow. An example of a radial decay showing the transition between inertia-capillary and elasto-capillary thinning is shown in Figure 9. From the data in Figure 9, one can independently determine the experimental transition radius, R^*, from the intersection of the inertia-capillary and elasto-capillary region of the radial decay and the relaxation time from the late stage exponential decay of the data.

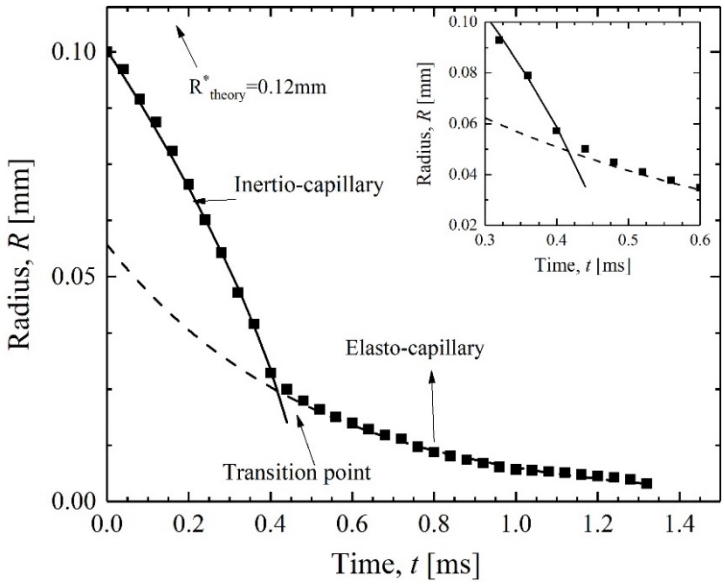

Figure 9. Radial decay, *R*, as a function of time, *t*, for the PEO of molecular weight M_w =1x10^6 g/mol in water at a reduced concentration of c/c^*=0.05 and shear viscosity of η_0=1 mPa.s (■) showing the transition from an inertia dominated thinning to an elasticity dominated thinning. Solid lines represents the inertial (—) and exponential fits (- -) to the experimental radius. An inset figure is provided with the magnified image to demonstrate the sharpness of the transition point.

By comparing the theoretical transition radius obtained from equation 7 and the experimentally determined transition radius, it can be seen from Figure 9 that the theoretical transition radius predictions was significantly larger than the experimentally measured value. From the data presented in Figure 9, for a PEO solution with $M_w = 1\times10^6$ g/mol, $\eta_0 = 1$ mPa.s and c/c^*=0.05, the transition radii were found to be $R^*_{theory} = 0.12$mm and $R^* = 0.022$mm. The magnitude of the theoretical over prediction in the transition radius was found to be consistent across molecular weight, shear viscosity and reduced concentration. If one takes the ratio of the experimental and theoretical transition radius, a correction factor can be found such that $\beta = R^* / R^*_{theory}$=0.18. Similar values of the correction factor, β, were observed for all the PEO solutions tested. The average correction factor for all the PEO solution data was found to be $\beta = 0.18 \pm 0.01$. The small size of the uncertainty in the correction factor data is remarkable given the data spans several orders of magnitude in M_w, η_0 and c/c^*. Additionally, it gives us confidence that an experimentally observed transition radius can be used to predict the relaxation time of low viscosity and low concentration PEO solution by capturing just a single data point. Rewriting equation 7 in terms of the experimentally observed transition radius, R^*, and theoretically and the average correction factor $\beta = 0.18$ as

$$\lambda_E = 13.1\left(\frac{R^{*3}\rho}{\sigma}\right)^{1/2} \tag{8}$$

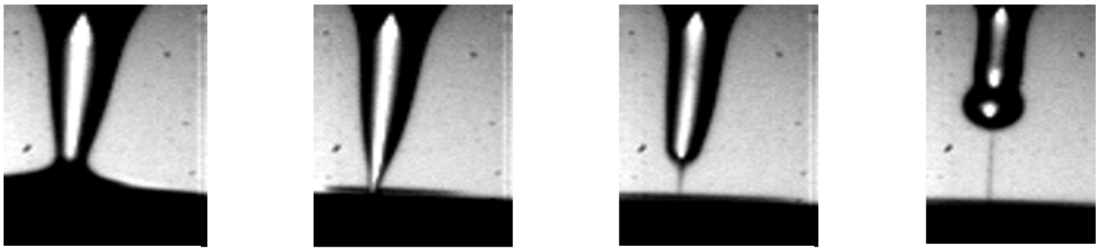

t=0.1ms *t*=0.14ms *t*=0.18ms *t*=0.22ms

Figure 10. Filament thinning dynamics of an aqueous solution of PEO with a molecular weight of M_w =200k g/mol at a reduced concentration of c/c^*=0.05 and a shear viscosity of η_0=1 mPa.s. Images were captured at 50,000 frames per seconds.

An example showing the power of this technique is shown in Figure 10 for CaBER-DoS breakup of a PEO with molecular weight of M_w =200k g/mol, and reduced concentration of c/c^*=0.05 in water with η_0=1 mPa.s. Note that in the images in Figure 10, the breakup of the fluid is in the inertia-capillary regime up until the last two frames. At time t = 0.18 ms, hints of a cylindrical filament can be seen and at t = 0.22 ms a clear cylindrical filament is produced. From those two images and the last $t = 40$ μs of the data, the relaxation time of the fluid can be calculated from equation 8. For this fluid, the extensional relaxation time was found to be $\lambda_E = 22$ μs. A similarly late stage cylindrical filament was observed for M_w =100k g/mol PEO in water at c/c*=0.08. For that solution, the extensional relaxation time calculated using equation 8 was found to be $\lambda_E = 20$ μs. To demonstrate the viability of our technique for that the relaxation time data for the 100k g/mol PEO solution was superimposed over the relaxation time data in Figure 3a obtained through the standard exponential fit to the time diameter decay data. As can be seen in Figure 3a, the relaxation time obtained with our experimental technique fits quite nicely in the trend line extrapolated from the higher relaxation time data. Given the maximum magnification of our high speed camera setup, the minimum resolvable radius can be used to

calculate a theoretical lower limit of the relaxation time can be determined directly from equation 8. For a solution with water as the solvent and a minimum radius of R_{min} = 5 μm equivalent to a single pixel, a minimum relaxation time of $\lambda_E = 17$ μs can be measured here. However, further improvements can be made with an increase in the magnification, speed, and resolution of the high speed camera and optics. Perhaps with increased improvements a better understandings of the differences observed between these extensional rheology measurements and the predictions of the Zimm theory can be obtained.

Although, the empirical correction factor β appears to do an adequate job at rectifying the observed differences between the observed transition radius and radius predicted by theory, it is desirable to obtain a better understanding of the origins of these differences and perhaps put them into a theoretical framework that allows us to derive β directly from theory. Here we direct the readers to an excellent paper by Wagner et al. [35]. In this paper, Wagner et al. [35] showed in great detail the transition between breakup regimes in CaBER measurements. Using a FENE-P constitutive model, they were able to calculate the diameter evolution and better understand transition between regimes. They demonstrated, that it is not the Weissenberg number that dictates the transition to elasto-capillary decay, but the level of the elastic extensional stresses. Beyond a Weissenbeg number of $Wi > 1/2$ elastic stresses are built up as strain is accumulated in the polymer chains in solution. Wagner et al. [35] demonstrated that the transition to elasto-capillary flow occurs when the elastic stresses become comparable in magnitude to the viscous and/or inertial contributions from the solvent. Using the FENE-P model, Wagner et al. [35] were able to derive an analytical solution for the transition radius and the transition time by considering the point at which the visco-capillary or inertia-capillary and elasto-capillary balances hold simultaneously. Their calculations were in excellent agreement to

their experimental data. It is important to note, however, that although this analysis is quite powerful when enough data is available in the elasto-capillary regime to fit the exponential decay and independently determine the values of the finite extensibility, *b*, plateau modulus, *G* and relaxation time, λ, for our experiments, where only a single data point is available in the elasto-capillary region, it is not possible to calculate the longest relaxation time using Wagner et al. [35] analysis without already knowing the elastic modulus and finite extensibility through other measurements. That being said, their work clearly explains the need for the correction factor, β, as the overshoot in the extension rates beyond $Wi=\lambda\dot{\varepsilon}$ >2/3 and the reduction in measured transition radius compared to theory was shown to be the direct result of the need to build up adequate elastic stress.

Using the CaBER-DoS technique, this overshoot in the extension rate beyond *Wi* = 2/3 can be studied and is presented in Figure 11a. The extension rate as a function of accumulated strain for three different concentration of PEO with M_w =200k g/mol is shown for a solution with shear viscosity of $\eta_0 = 6$ mPa.s. The first observation is that the extension rate observed for all three solutions was found to overshoot well past *Wi*=2/3. In all cases, *Wi*=2 was achieved before sufficient elastic stress was built up in the filament to slow the extension rate slowed back to the expected CaBER value of *Wi*=2/3. The form of the extension rate variation with time for the three cases presented in Figure 11 and in fact all the cases studied was quite similar. If the data were normalized with relaxation time and replotted as *Wi*, they quite nearly collapse into a single curve as shown in the inset of Figure 11a. The form was also consistent with changes in molecular weight and solvent viscosity. As seen in Figure 11b, the magnitude of extension rate overshoot was found to increase linearly with the inverse of relaxation time of the solutions. The average Weissenberg number observed during the extension rate overshoot for all the PEO

solutions tested was found to be $Wi_{averge} = 1.7 \pm 0.1$. From our parametric study it has also been observed that the average Hencky strain accumulated during the extension rate overshoot was

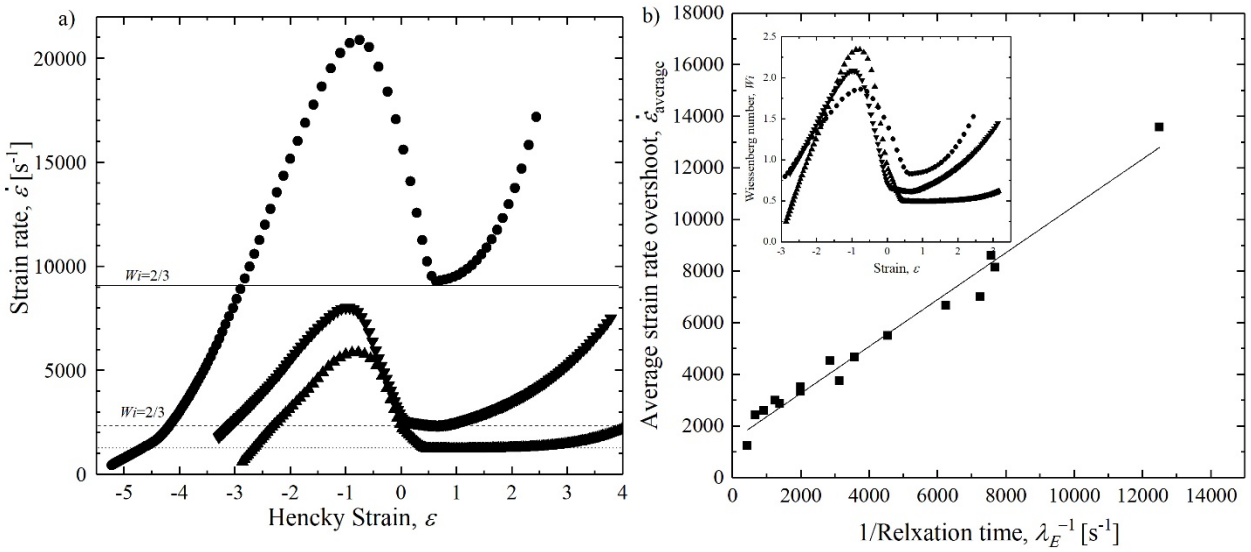

$\varepsilon_{average} = 3$. This strain accumulated during the overshoot account for the difference between the theoretical and experimentally measured transition radii.

Figure 11. (a) Plot of the extension rate, $\dot{\varepsilon}$ as a function of Hencky strain, ε, for a PEO solution with molecular weight of M_w =200k g/mol at reduced concentrations of c/c^*=0.05 (●), c/c^*=0.1 (▼) and c/c^*=0.5 (▲) and shear viscosity of η_0=6 mPa.s showing the overshoot beyond the expected Wi=2/3 decay at the transition from the inertia-capillary to the elasto-capillary regimes. Horizontal lines represents the Weissenberg number Wi=2/3 for c/c*=0.05 (solid line), c/c^*=0.1 (--) and c/c^*=0.5 (··), (b) Plot of the average extension rate overshoot, $\dot{\varepsilon}_{average}$, as a function of inverse of relaxation time, $1/\lambda_E$, for a series of PEO solution in glycerin and water with varying molecular weight, solution viscosity and reduced concentration. The inset Figure in 11b shows the plot of Weissenberg number, Wi as a function of strain, ε.

VII Conclusion

The filament breakup process of a series of dilute PEO solutions of varying molecular weight, shear viscosity and reduced concentration using the Dripping onto Substrate Capillary Breakup Extensional Rheometry (CaBER-DoS) was investigated. For the low viscosity fluids, at

early times during the stretch viscous and elastic stresses are irrelevant for Wi<1/2 and thus the dynamics are controlled by the inertia-capillary balance. However, as the time approaches the cutoff time $t_{c,}$ the extension rate can grow large enough such that Wi >1/2 and as a result of this significant polymer chain extension, the elastic stresses grows to match the capillary pressure, preventing the neck from breaking off. In CaBER-DoS, the stretching happens at a constant extension rate of $\dot{\varepsilon} = 2/3\lambda$. Scaling laws were established for the variation of extensional relaxation time as a function of reduced concentration, molecular weight and solution shear viscosity. The extensional relaxation time, λ_E was calculated through an exponential fit to the diameter decay data in the elasto-capillary thinning regime. In order for this fit to be accurate, a minimum of 5-10 data points is required. Most of the trends were found to be in accordance with the theory and thus these scaling relations can be used for extrapolating data for low viscosity, concentration and molecular weight PEO solutions. However, unlike the predictions of theory the measured extensional relaxation time at extremely low concentration did not agree with the predictions of Zimm theory, but significantly under predicted it.

As discussed in earlier sections, this transition from an initial power law decay to the late stage exponential decay was found to be extremely sharp. By taking advantage of this sharp transition, the resolution and sensitivity of the CaBER-DoS technique were significantly enhanced and extensional relaxation time close to ten microseconds was measured within the limits of the spatial and temporal resolution of our optics and high speed camera. A consistent correction factor $\beta = R^* / R^*_{theory} = 0.18$ was found using the experiments performed on high viscosity and molecular weight PEO solutions. Here, R^* is the experimental transition radius and R^*_{theory} is the theoretical transition radius. Using this correction factor an empirical relation was derived which was used to predict the extensional relaxation time of low viscosity and low

concentration PEO solution by capturing just a single image showing a cylindrical filament. The minimum extensional relaxation time that was calculated using the correction factor β for one of our experiments on a PEO solution was found to be $\lambda_E = 20\ \mu s$. Through our empirical relation the lower limit of the minimum measured extensional relaxation time available in the literature was further pushed but further improvements are still required so that full characterization of ultra-dilute solution with smaller and smaller relaxation times can be characterized.

Supplementary Material

See supplementary material for the complete details about the shear viscosity and surface tension data of each solution tested in the paper.

Acknowledgements

Authors would like to thank Christian Clasen of KU Leuven for use of his Edgehog software and Vivek Sharma of UIC (Chicago) for inspiration behind the CaBER experiments.

References

[1] McKinley, G. H., and T. Sridhar, ‘‘Filament-stretching rheometry of complex fluids,’’ Annual Review of Fluid Mechanics 34, 375-415 (2002).

[2] Clasen, C., J. Plog, W.-M. Kulicke, M. Owens, C. Macosko, L. Scriven, M. Verani, and G. H. McKinley, ‘‘How dilute are dilute solutions in extensional flows,’’ Journal of Rheology 50, 849-881 (2006).

[3] Entov, V., and A. Yarin, ‘‘Influence of elastic stresses on the capillary breakup of jets of dilute polymer solutions,’’ Journal of Fluid Dynamics 19, 21-29 (1984).

[4] Kolte, M. I., and P. Szabo, ‘‘Capillary thinning of polymeric filaments,’’ Journal of Rheology 43, 609-625 (1999).

[5] McKinley, G. H., ‘‘Visco-elasto-capillary thinning and break-up of complex fluids,’’ (2005).

[6] Rodd, L. E., T. P. Scott, J. J. Cooper-White, and G. H. McKinley, ‘‘Capillary break-up rheometry of low-viscosity elastic fluids,’’ Journal Of Applied Rheology (2004).

[7] Tirtaatmadja, V., G. H. McKinley, and J. J. Cooper-White, ‘‘Drop formation and breakup of low viscosity elastic fluids: Effects of molecular weight and concentration,’’ Physics of Fluids 18, 043101 (2006).

[8] Morrison, N. F., and O. G. Harlen, ‘‘Viscoelasticity in inkjet printing,’’ Rheologica Acta 49, 619-632 (2010).

[9] Lampe, J., R. DiLalla, J. Grimaldi, and J. P. Rothstein, ‘‘Impact dynamics of drops on thin films of viscoelastic wormlike micelle solutions,’’ Journal of Non-Newtonian Fluid Mechanics 125, 11-23 (2005).

[10] Dinic, J., Y. Zhang, L. N. Jimenez, and V. Sharma, ‘‘Extensional relaxation times of dilute, aqueous polymer solutions,’’ ACS Macro Letters 4, 804-808 (2015).

[11] Dinic, J., L. N. Jimenez, and V. Sharma, ‘‘Pinch-off dynamics and dripping-onto-substrate (dos) rheometry of complex fluids,’’ Lab on a Chip 17, 460-473 (2017).

[12] Kolte, M. I., H. K. Rasmussen, and O. Hassager, ‘‘Transient filament stretching rheometer,’’ Rheologica Acta 36, 285-302 (1997).

[13] Szabo, P., ‘‘Transient filament stretching rheometer,’’ Rheologica Acta 36, 277-284 (1997).

[14] Anna, S. L., G. H. McKinley, D. A. Nguyen, T. Sridhar, S. J. Muller, J. Huang, and D. F. James, ‘‘An interlaboratory comparison of measurements from filament-stretching rheometers using common test fluids,’’ Journal of Rheology 45, 83-114 (2001).

[15] Tirtaatmadja, V., and T. Sridhar, ‘‘A filament stretching device for measurement of extensional viscosity,’’ Journal of Rheology 37, 1081-1102 (1993).

[16] Spiegelberg, S. H., D. C. Ables, and G. H. McKinley, ‘‘The role of end-effects on measurements of extensional viscosity in filament stretching rheometers,’’ Journal of Non-Newtonian Fluid Mechanics 64, 229-267 (1996).

[17] Bach, A., H. K. Rasmussen, and O. Hassager, ‘‘Extensional viscosity for polymer melts measured in the filament stretching rheometer,’’ Journal of Rheology 47, 429-441 (2003).

[18] Anna, S. L., and G. H. McKinley, ‘‘Elasto-capillary thinning and breakup of model elastic liquids,’’ Journal of Rheology 45, 115-138 (2001).

[19] Vadillo, D. C., W. Mathues, and C. Clasen, ‘‘Microsecond relaxation processes in shear and extensional flows of weakly elastic polymer solutions,’’ Rheologica Acta 51, 755-769 (2012).

[20] Campo-Deano, L., and C. Clasen, ‘‘The slow retraction method (srm) for the determination of ultra-short relaxation times in capillary breakup extensional rheometry experiments,’’ Journal of Non-Newtonian Fluid Mechanics 165, 1688-1699 (2010).

[21] Vadillo, D., T. Tuladhar, A. Mulji, S. Jung, S. Hoath, and M. Mackley, ‘‘Evaluation of the inkjet fluid’s performance using the “cambridge trimaster” filament stretch and break-up device,’’ Journal of Rheology 54, 261-282 (2010).

[22] Greiciunas, E., J. Wong, I. Gorbatenko, J. Hall, M. Wilson, N. Kapur, O. Harlen, D. Vadillo, and P. Threlfall-Holmes, ‘‘Design and operation of a rayleigh ohnesorge jetting extensional rheometer (rojer) to study extensional properties of low viscosity polymer solutions,’’ Journal of Rheology 61, 467-476 (2017).

[23] Keshavarz, B., V. Sharma, E. C. Houze, M. R. Koerner, J. R. Moore, P. M. Cotts, P. Threlfall-Holmes, and G. H. McKinley, ‘‘Studying the effects of elongational properties on atomization of weakly viscoelastic solutions using rayleigh ohnesorge jetting extensional rheometry (rojer),’’ Journal of Non-Newtonian Fluid Mechanics 222, 171-189 (2015).

[24] Muthukumar, M., ‘‘Concentration dependent relaxation times of linear polymers in dilute solutions,’’ Macromolecules 17, 971-973 (1984).

[25] Dinic, J., L. N. Jimenez, and V. Sharma, ‘‘Pinch-off dynamics and dripping-onto-substrate (dos) rheometry of complex fluids,’’ Lab on a Chip (2017).

[26] Graessley, W. W., “The entanglement concept in polymer rheology.” *The entanglement concept in polymer rheology* (Springer, 1974).

[27] Takamura, K., H. Fischer, and N. R. Morrow, ‘‘Physical properties of aqueous glycerol solutions,’’ Journal of Petroleum Science and Engineering 98, 50-60 (2012).

[28] Mun, R. P., J. A. Byars, and D. V. Boger, ‘‘The effects of polymer concentration and molecular weight on the breakup of laminar capillary jets,’’ Journal of Non-Newtonian Fluid Mechanics 74, 285-297 (1998).

[29] Clasen, C., P. M. Phillips, and L. Palangetic, ‘‘Dispensing of rheologically complex fluids: The map of misery,’’ AIChE Journal 58, 3242-3255 (2012).

[30] Papageorgiou, D. T., ‘‘On the breakup of viscous liquid threads,’’ Physics of Fluids 7, 1529-1544 (1995).

[31] Entov, V. M., and E. J. Hinch, ‘‘Effect of a spectrum of relaxation times on the capillary thinning of a filament of elastic liquid,’’ J. Non-Newtonian Fluid Mech. 72, 31-53 (1997).

[32] Wagner, C., L. Bourouiba, and G. H. McKinley, ‘‘An analytic solution for capillary thinning and breakup of fene-p fluids,’’ J. Non-Newt. Fluid Mech 218, 53-61 (2015).

[33] Rubinstein, M., and R. H. Colby, Polymer physics Vol. 23 (Oxford university press New York, 2003).

[34] Bazilevskii, A., V. Entov, and A. Rozhkov, ‘‘Breakup of an oldroyd liquid bridge as a method for testing the rheological properties of polymer solutions,’’ Polymer Science Series Of Vysokomolekuliarnye Soedineniia 43, 716-726 (2001).

[35] Wagner, C., L. Bourouiba, and G. H. McKinley, ‘‘An analytic solution for capillary thinning and breakup of fene-p fluids,’’ Journal of Non-Newtonian Fluid Mechanics 218, 53-61 (2015).